J Mater Sci (2008) 43:832–838
DOI 10.1007/s10853-007-2195-4

Preparation and sintering behaviour of a fine grain $BaTiO_3$ powder containing 10 mol% $BaGeO_3$

Roberto Köferstein · Lothar Jäger · Mandy Zenkner · Hans-Peter Abicht

Received: 25 July 2007 / Accepted: 27 September 2007 / Published online: 31 October 2007

Abstract The formation of solid solutions of the type $[Ba(HOC_2H_4OH)_4][Ti_{1-x}Ge_x(OC_2H_4O)_3]$ as $Ba(Ti_{1-x}/Ge_x)O_3$ precursors and the phase evolution during thermal decomposition of $[Ba(HOC_2H_4OH)_4][Ti_{0.9}Ge_{0.1}(OC_2H_4O)_3]$ (**1**) are described herein. The 1,2-ethanediolato complex **1** decomposes above 589 °C to a mixture of $BaTiO_3$ and $BaGeO_3$. A heating rate controlled calcination procedure, up to 730 °C, leads to a nm-sized $Ba(Ti_{0.9}/Ge_{0.1})O_3$ powder (**1a**) with a specific surface area of $S = 16.9$ m^2/g, whereas a constant heating rate calcination at 1,000 °C for 2 h yields a powder (**1b**) of $S = 3.0$ m^2/g. The shrinkage and sintering behaviour of the resulting $Ba(Ti_{0.9}/Ge_{0.1})O_3$ powder compacts in comparison with nm-sized $BaTiO_3$ powder compacts (**2a**) has been investigated. A two-step sintering procedure of nm-sized $Ba(Ti_{0.9}/Ge_{0.1})O_3$ compacts (**1a**) leads, below 900 °C, to ceramic bodies with a relative density of ≥90%. Furthermore, the cubic ⇆ tetragonal phase transition temperature has been detected by dilatometry, and the temperature dependence of the dielectric constant (relative permittivity) has also been measured.

Introduction

Barium titanate ($BaTiO_3$) is one of the most frequently used ceramic materials in electronics due to its dielectric properties. The sintering temperature of $BaTiO_3$, prepared by conventional mixed-oxide method, is in general, considerably above 1,200 °C to obtain dense ceramic bodies [1]. Sintering temperatures of about 1,100 °C are possible using nano-sized $BaTiO_3$ and a two-step sintering procedure [2]. Some additives, like SiO_2 or lead germanate, can reduce the sintering temperature [3–5]. Pulvari [6] and Baxter et al. [7] gave the first summary of additives and their influence on the properties of $BaTiO_3$. Additives can influence not only the sintering temperature, but also the dielectric/electrical properties of the final ceramics [8, 9]. The addition of germanates, like lead germanate, are used in industrial applications to produce heterophasic ceramic bodies [10, 11]. Up to now, the influence of $BaGeO_3$ on the sintering behaviour and properties of $BaTiO_3$ has rarely been investigated. To date, only Guha [12] has examined the $BaO–TiO_2–GeO_2$ system and observed two ternary compounds ($BaTiGe_3O_9$, $Ba_2TiGe_2O_8$). Furthermore, Guha and Kolar [13] studied the $BaTiO_3–BaGeO_3$ system, and they determined a eutectic composition of 68 mol% $BaGeO_3$ with a melting temperature of about 1,120 ± 5 °C. Additionally, they observed no shifting of the cubic ⇆ tetragonal phase transition temperature of $BaTiO_3$ (Curie temperature) by addition of $BaGeO_3$, as is consistent with the investigation by Plessner and West [14]. Plessner and West noticed only a reduction of the sharpness of the permittivity maximum. In contrast, Pulvari [6] and Baxter [7] found a small decrease in the Curie temperature with the addition of GeO_2.

This publication reports on fine grain barium titanate powder containing 10 mol% barium germanate by decomposition of a barium titanium germanium 1,2-ethanediolato complex. In addition, the shrinkage and sintering behaviour of resulting powder compacts and also the dielectric properties of ceramic bodies have been investigated.

R. Köferstein · L. Jäger · M. Zenkner · H.-P. Abicht (✉)
Institute of Chemistry/Inorganic Chemistry, Martin-Luther-University Halle-Wittenberg, 06099 Halle, Germany
e-mail: hans-peter.abicht@chemie.uni-halle.de

Experimental

Material preparation

$[Ba(HOC_2H_4OH)_4][Ti_{0.9}Ge_{0.1}(OC_2H_4O)_3]$ (**1**) was prepared analogous to the preparation of $[Ba(HOC_2H_4OH)_4][Ti(OC_2H_4O)_3]$ (**2**) [15]. However, 10 mol% of the quantity of $Ti(O^iC_3H_7)_4$ was substituted by $Ge(OC_2H_5)_4$. The product was a white, hygroscopic solid. Yield: >95%.

Analysis: $C_{14}H_{36}O_{14}BaTi_{0.9}Ge_{0.1}$ (616.11 g/mol): calc. C, 27.29%; H, 5.89%, found C, 27.27%; H, 5.95%.

1 was calcined at 1,000 °C for 2 h to determine the Ba^{2+}, Ti^{4+} and Ge^{4+} content. The powder that resulted (290 mg) was dissolved in a solution of 20 mL H_2O_2 (30%) and 4 mL $HClO_4$ (70%) at 40–50 °C. The amounts of Ba^{2+}, Ti^{4+} and Ge^{4+} were determined by atomic absorption spectroscopy (AAS), colorimetry, gravimetric analysis and chelatometric titration [16–18]. The analyses indicated a Ba/Ti ratio of 1.117 and a Ba/(Ti + Ge) ratio of 0.999. These values correspond very well with the expected values.

Ba(Ti/Ge)-precursors with different Ti/Ge ratios were prepared analogous to **1**.

For the shrinkage and sintering behaviour, the calcined powders were milled and pressed to disks (green density: 2.8–2.9 g/cm^3), as described in [19].

Analytical methods

X-ray powder diffraction (XRD) patterns were recorded by a STADI MP diffractometer from *STOE* (Germany) at 25 °C using CoKα_1 radiation, and a step size of 0.03° for 2θ. Simultaneous thermogravimetric (TG) and differential thermoanalytic (DTA) measurements were achieved using a STA 429 from *Netzsch* (Germany, Pt crucible, flowing air (75 mL/min)). The dilatometric investigations (shrinkage) were performed in a TMA 92-16.18 unit from *Setaram* (France), and the densities of the discs were calculated assuming an isotropic shrinkage behaviour. The specific surface area was measured using nitrogen three-point BET (Nova 1000, *Quantachrome Corporation*, USA). The average particle size was calculated assuming the powder particles were spherical or cubic in shape. Crystallite sizes were determined by XRD line broadening using the Scherrer equation [20] and the integral peak breadth. Measurements of the dielectric constants at 1 kHz were achieved using an Impedance Analyzer 4192 Alf from *Hewlett Packard* (USA) and a temperature rate of 0.3 K/min. An analyzer CHNS 932 (*LECO Instruments GmbH*) was used for elemental analyses. Atomic absorption spectroscopy (AAS) was performed using a *Varian* Spectra 20 instrument. Scanning electron microscope images were recorded with a *Philips* XL30 ESEM (Environmental Scanning Electron Microscope).

Results and discussion

Solid solutions of the type $[Ba(HOC_2H_4OH)_4][Ti_{1-x}Ge_x(OC_2H_4O)_3]$

Recently, we have reported on the 1,2-ethanediolato complexes $[Ba(HOC_2H_4OH)_4][Ti(OC_2H_4O)_3]$ (**2**) and $[Ba(HOC_2H_4OH)_2Ge(OC_2H_4O)_3]$ (**3**) as precursors for $BaTiO_3$ and $BaGeO_3$ ceramics [15, 19, 21]. Indeed, these complexes **2** and **3** are not isotypic. However, XRD investigations suggest that the reaction of $Ba(OH)_2 \cdot 8H_2O$ with $Ti(O^iC_3H_7)_4$ and $Ge(OC_2H_5)_4$ in boiling 1,2-ethanediol leads to solid solutions of the type $[Ba(HOC_2H_4OH)_4][Ti_{1-x}Ge_x(OC_2H_4O)_3]$ up to a germanium content of $x \approx 0.2$. XRD patterns of some precursor complexes with different Ti/Ge ratios can be seen in Fig. 1. The XRD diagrams of some $[Ba(HOC_2H_4OH)_4][Ti_{1-x}Ge_x(OC_2H_4O)_3]$ precursor complexes ($0 \leq x \leq 0.2$) show only the reflexion pattern of complex **2** (Fig 1b–d). This observation indicates that each sample consists of a single phase and suggests the formation of solid solutions of the type $[Ba(HOC_2H_4OH)_4][Ti_{1-x}Ge_x(OC_2H_4O)_3]$. Furthermore, the insertion of Ge^{4+} into the crystal structure of **2** is connected to a decrease in unit cell volume (inset in Fig. 1). As exemplified in Fig. 1e, a further increase in the germanium content in the reaction solution (Ti/Ge > 0.2) leads to the appearance of an

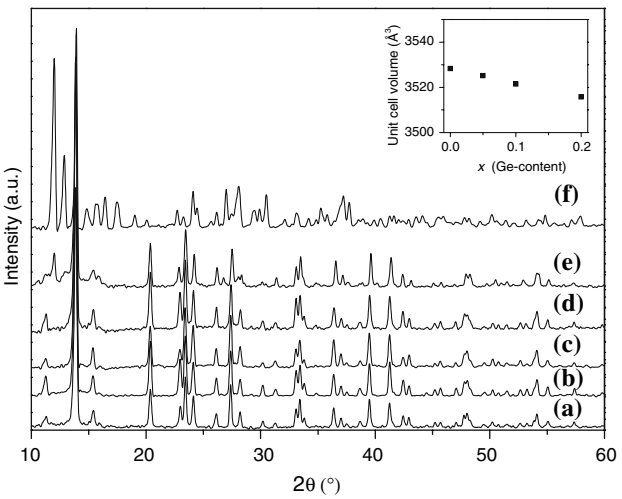

Fig. 1 XRD patterns of (a) $[Ba(HOC_2H_4OH)_4][Ti(OC_2H_4O)_3]$ (**2**), (b–d) $[Ba(HOC_2H_4OH)_4][Ti_{1-x}Ge_x(OC_2H_4O)_3]$ (b) $x = 0.05$, (c) $x = 0.1$, (d) $x = 0.2$), (e) consecutive product of a reaction, in which 50 mol% of $Ti(O^iC_3H_7)_4$ were substituted by $Ge(OC_2H_5)_4$, (f) $[Ba(HOC_2H_4OH)_2Ge(OC_2H_4O)_3]$ (**3**). The inset shows the relationship between the volume of the unit cell and the germanium content (x) of some $[Ba(HOC_2H_4OH)_4][Ti_{1-x}Ge_x(OC_2H_4O)_3]$ complexes

additional crystalline phase. The reflexions of that second phase at $2\theta \approx 12.0$, 12.9 and 15.8° represent the formation of complex **3** [19].

Figure 2 shows XRD patterns of $[Ba(HOC_2H_4OH)_4][Ti_{0.9}Ge_{0.1}(OC_2H_4O)_3]$ (**1**) after different calcination steps (dwelling time 1 h). A calcination temperature of 500 °C leads to a diffraction pattern with reflexions belonging to an intermediate phase, as described in [22, 23], and reflexions of $BaTiO_3$ and orthorhombic $BaCO_3$ [24]. Calcination at 700 °C results in the formation of a (pseudo)-cubic $BaTiO_3$ phase and small amounts of $BaCO_3$. Heat treatment at 1,000 °C causes a weak splitting of the peak at about $2\theta \approx 52.8°$ into the (002) and (200) peaks indicating the transformation from cubic to tetragonal $BaTiO_3$. Powders calcined above 800 °C show weak peaks belonging to orthorhombic $BaGeO_3$ and Ba_2GeO_4 [24]. Consequently, the calcination of **1** does not lead to a solid solution of the type $BaTi_{0.9}Ge_{0.1}O_3$, as was also found to be the case in the investigations by Guha and Kolar [13]. They reported that only up to about 1.8 mol% Ge^{4+} (related to the occupation of the Ti^{4+} site) is incorporated into the $BaTiO_3$ structure. Therefore, the calcination product of **1** is predominantly a mixture of barium titanate and barium germanate (0.9 $BaTiO_3$/0.1 $BaGeO_3$). In this article, we describe that mixture by the formula $Ba(Ti_{0.9}/Ge_{0.1})O_3$.

TG/DTA investigations of $[Ba(HOC_2H_4OH)_4][Ti_{0.9}Ge_{0.1}(OC_2H_4O)_3]$ (**1**)

Figure 3 shows the TG and DTA curves for **1** in flowing air with a heating rate of 10 and 1 K/min, respectively. Figure 3a (heating rate 10 K/min) shows two endothermic peaks beginning (T_{onset}) at about 117 °C and 144 °C. The

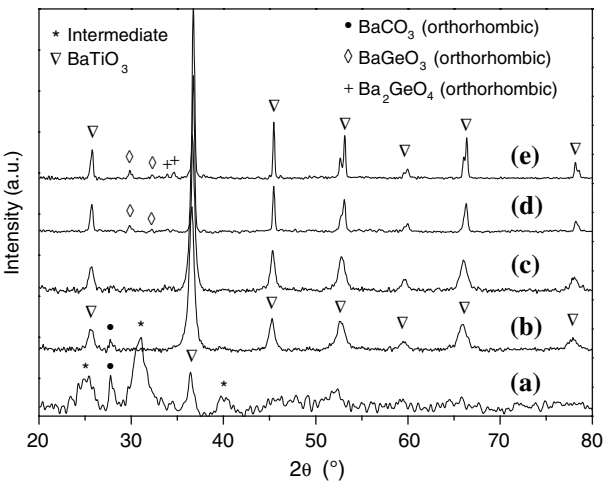

Fig. 2 XRD patterns of **1** calcined at different temperatures in static air (heating/cooling rate 10 K/min, dwelling time 1 h), (a) 500 °C, (b) 700 °C, (c) 800 °C, (d) 1,000 °C, (e) 1,100 °C

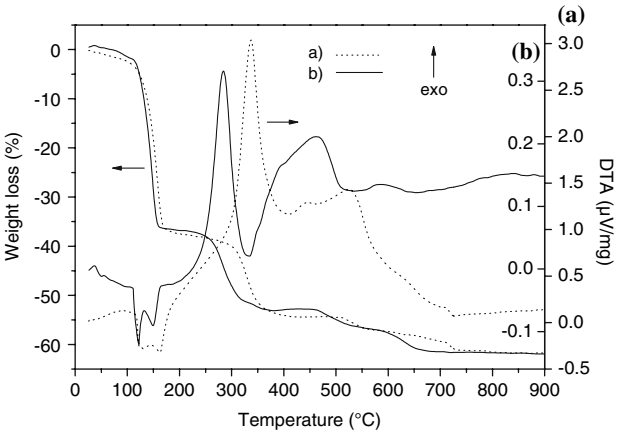

Fig. 3 TG and DTA curves of **1** in flowing air, (a) heating rate 10 K/min, (b) heating rate 1 K/min

resulting weight loss until 196 °C is due the loss of solvate molecules (39.2%). A further weight loss, starting at 283 °C, leads to a total weight loss of 54.4%, and is accompanied by an exothermic decomposition process (T_{onset}: 306 °C). The observed intermediate state is stable up to about 510 °C. After several weight losses, the last stage of decompositions starts at 705 °C, and the formation of $Ba(Ti_{0.9}/Ge_{0.1})O_3$ is complete by 795 °C. The total weight loss of 61.5% is in excellent agreement with the theoretical value of 61.7%.

A comparison between the TG/DTA analyses with heating rates of 10 and 1 K/min (Fig. 3a, b) shows that the beginning of the several decomposition stages strongly depends on the heating rate. In particular, the final stage of decomposition is shifted to a lower temperature by a heating rate of 1 K/min. Here, the final stage starts at 589 °C, and the precursor is completely transformed into $Ba(Ti_{0.9}/Ge_{0.1})O_3$ by about 716 °C. Similar observations during the decomposition of $BaTiO(C_2O_4)_2 \cdot 4H_2O$ are reported by Polotai et al. [25].

The calcination regime (temperature, heating rate and dwelling time) has a great influence on the resulting particle size. Lower calcination temperatures lead to powders with higher specific surface areas and smaller particles [15, 26]. According to the thermal analyses, **1** was calcined by the following thermal treatment: heating to 550 °C with a heating rate of 10 K/min, slow heating with 1 K/min to 730 °C, dwelling time 30 min and followed by cooling at 10 K/min. The resulting powder contains only traces of $BaCO_3$. This thermal treatment leads to a $Ba(Ti_{0.9}/Ge_{0.1})O_3$ powder (**1a**) with a specific surface area of $S = 16.9\ m^2/g$ and an average particle size of $d_{avar.} = 61$ nm. Crystallite-size measurement by XRD line broadening [20] of the (111) reflexion of the $BaTiO_3$ phase reveals a lower value of about $d_{crys.} = 40$ nm. The XRD line broadening indicates only a crystallite size of the $BaTiO_3$ phase, whereas

the specific surface area indicates an average particle size of all phases including agglomerates. Moreover, the decomposition leads to the development of an internal surface in the powder (closely joined crystallites), which is unavailable for nitrogen adsorption. Analogous discrepancies between the particle-/crystallite-size estimated by the XRD line broadening and the specific surface area were also observed in studies of ThO_2 and ZrO_2 [27, 28].

Shrinkage and sintering behaviour

Three different preceramic powders were used for these investigations. Powder **1a** ($Ba(Ti_{0.9}/Ge_{0.1})O_3$) was obtained after calcination of precursor **1** at 730 °C, as described above (S = 16.9 m^2/g, $d_{avar.}$ = 61 nm), while powder **1b** ($Ba(Ti_{0.9}/Ge_{0.1})O_3$) is the resulting decomposition product of precursor **1** calcined at 1000 °C for 2 h with a heating rate of 10 K/min (S = 3.0 m^2/g, $d_{avar.}$ = 341 nm). Powder **2a** ($BaTiO_3$) was obtained by decomposition of precursor **2** with the same thermal treatment, as described for **1a** (Ba/Ti = 1.004, S = 15.0 m^2/g, $d_{avar.}$ = 66 nm). The theoretical bulk density of $Ba(Ti_{0.9}/Ge_{0.1})O_3$ ceramics was calculated as 5.85 g/cm^3 [19, 29, 30]. Besides the tetragonal $BaTiO_3$ phase, the $Ba(Ti_{0.9}/Ge_{0.1})O_3$ ceramic bodies mainly consist of hexagonal $BaGeO_3$ or $Ba_2TiGe_2O_8$ (as shown below in Fig. 7). The theoretical density of $BaTiO_3$ ceramics is 6.02 g/cm^3 [31]).

Figure 4 shows the dilatometric (non-isothermal) investigations of these three different powder compacts. Sample **1a**: a strong shrinkage process starts at about 790 °C, and the relative shrinkage rate reaches a maximum at 908 °C. Above 1,000 °C, a second shrinkage process can be observed. An increase in the shrinkage up to 1,170 °C leads to a maximum of the relative bulk density of 96% (5.60 g/cm^3) with respect to the theoretical density. Further heating results in a slight expansion of the sintered body, and thus in a decrease in density. The investigation of the shrinkage mechanism will be a subject for further studies.

The shrinkage curve of **1b** reveals, in particular, the influence of the particle size on the shrinkage behaviour. The beginning of the shrinkage process is shifted to a higher temperature. The sample begins to shrink slowly at 850 °C, and a first broad maximum of the shrinkage rate is reached at about 1,058 °C. A second strong shrinkage process begins at 1,110 °C, whereas the maximum of the shrinkage rate is observed at 1,164 °C. The last process is probably initiated by the formation of a liquid phase. Guha and Kolar [13] observed the formation of a liquid phase in the $BaTiO_3$–$BaGeO_3$ system at 1,120 ± 5 °C (eutectic temperature). At 1,400 °C, a relative density of 89% (5.23 g/cm^3) is reached.

A comparison of sample **1a** and **2a** shows the influence of $BaGeO_3$ on the shrinkage process. Both samples consist of comparable particle sizes (61 nm (**1a**), 66 nm (**2a**)). The sample **2a** slowly begins to shrink at about 800 °C, but a clear shrinkage process begins at 900 °C and shows two maxima of the shrinkage rate at 922 °C and 1,050 °C. The shrinkage curve of **2a** reveals an increasing densification at the end of the heating period and reaches 89% (5.38 g/cm^3) of the theoretical density.

Figure 5 shows the bulk densities of ceramic bodies of **1a** after conventional sintering (heating up to a certain temperature (rate 10 K/min), dwelling at this temperature and then cooling down with 10 K/min). The bulk densities of the sintered bodies were calculated from their weight and geometric dimensions. We obtain dense ceramic bodies below the formation of a liquid phase. It can be seen that a dwelling time of 1 h at 1,000 °C leads to dense

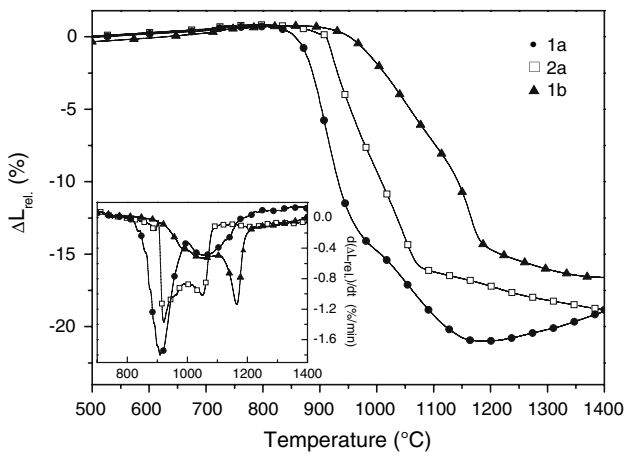

Fig. 4 The shrinkage behaviour up to 1,400 °C (heating rate 10 K/min, flowing air) of green bodies of **1a**, **2a** and **1b**, respectively. The inset shows the shrinkage rate of these bodies. ($\Delta L_{rel.} = \Delta L/L_0$)

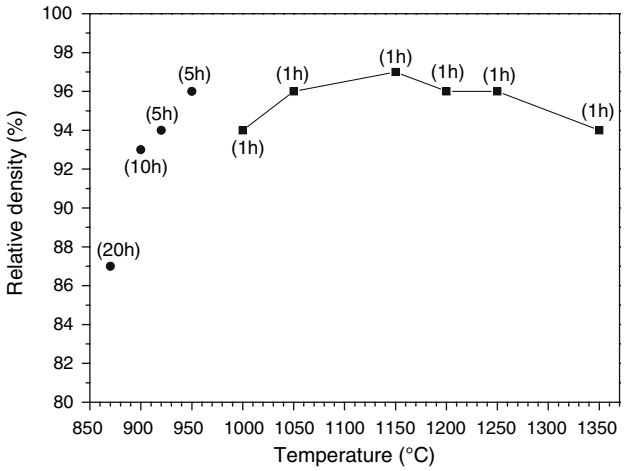

Fig. 5 Final densities of sintered bodies of **1a** after a conventional sintering procedure at the indicated dwelling times. The theoretical density was calculated to 5.85 g/cm^3

ceramic bodies (94%, 5.52 g/cm^3) and reaches, at 1,150 °C, a relative density of 97%. We observe a heterogeneous grain size distribution (Fig. 6a–c). The grain size of a ceramic body sintered at 1,000 °C is in the range of about 0.8–3.7 µm and at 1,100 °C, 1.5–5 µm. As the result of the formation of the liquid phase, we find a bi-modal grain size distribution with grain sizes of 5–40 µm (1,250 °C) and 11–60 µm (1,350 °C). It can be seen that the grains are surrounded by a solidified liquid phase. Analogous to the dilatometric investigation, sintering above 1,150 °C causes a small decrease in density. This so-called dedensification or desintering process is caused by an increase in volume of the body (see also Fig. 4). The dedensification of $BaTiO_3$ and other ceramics has been reported in several articles [9, 32–36]. Demartin et al. [32, 34] attributed the dedensification process to a bi-modal grain growth in dense ceramic bodies along with the appearance of a liquid phase. According to these studies, we obtain dense ceramic bodies (below 1,120 °C), which are characterized by a bi-modal grain size distribution, and the dedensification process takes place with the formation and spreading of the liquid phase. In contrast, powder compacts of **1b** do not show any dedensification processes (see Fig. 4) because of their lower densification. The dilatometric investigations reveal a relative density of 67% for **1b** (cp. 91% for **1a**) at 1,120 °C, and also a sintered body of **1b** with a relative density of 75% (1,090 °C, 1 h) shows a porous microstructure without any evidence of a bi-modal grain size distribution.

Additionally, dense ceramic bodies can be obtained below a sintering temperature of 1,000 °C by a prolonged dwelling time or a two-step sintering procedure [37]. A relative density of 93% can be observed by conventional sintering at 900 °C for 10 h. The resulting ceramic body consists of grains between about 0.7–4.8 µm in diameter (Fig. 6d).

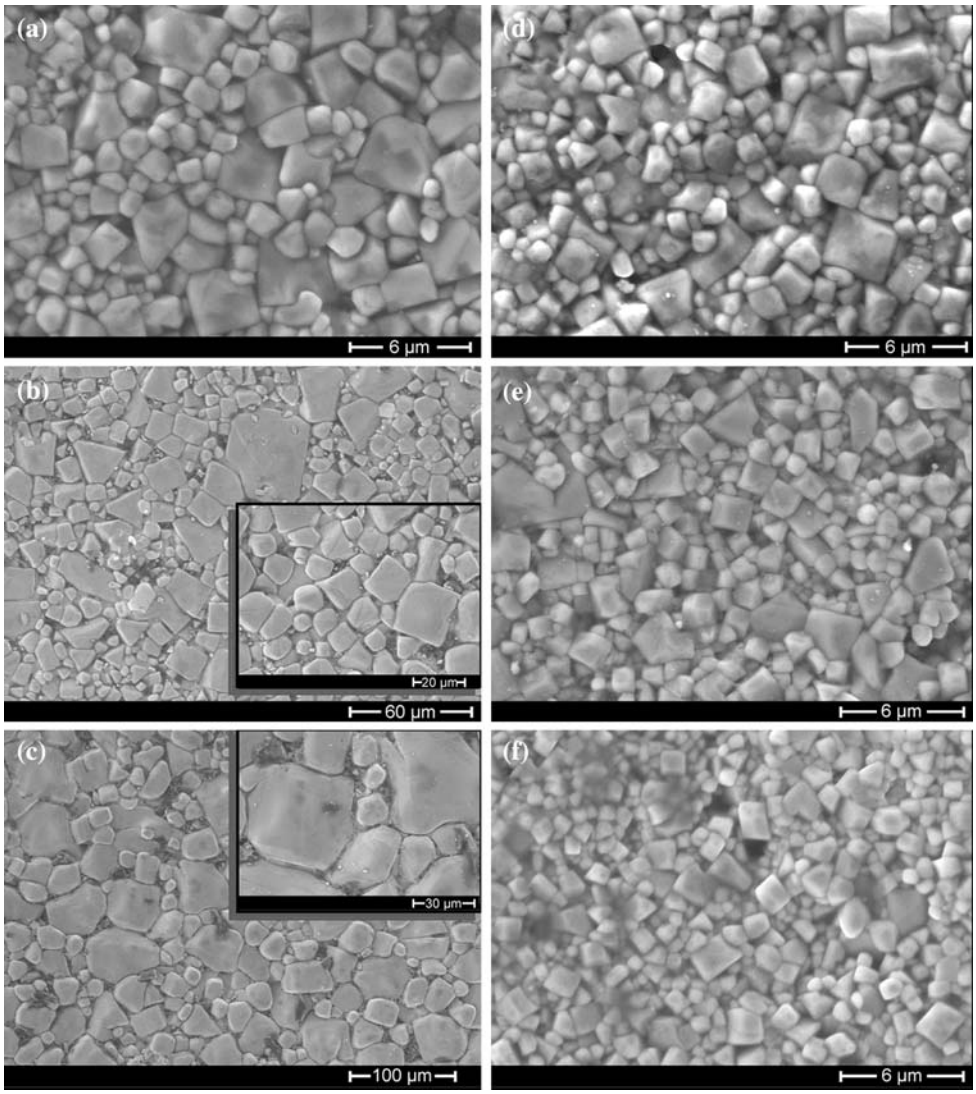

Fig. 6 SEM micrographs of the surfaces of ceramic bodies (**1a**) after different sintering procedures. (1) Conventional sintering, (**a**) 1,000 °C, 1 h; (**b**) 1,250 °C, 1 h; (**c**) 1,350 °C, 1 h; (**d**) 900 °C, 10 h. (2) two-step sintering procedure (dwelling time 50 h), (**e**) $T_1 = 950$ °C, $T_2 = 850$ °C, (**f**) $T_1 = 970$ °C, $T_2 = 840$ °C

As shown by Chen and Wang [37], a two-step sintering process can suppress the final-stage grain growth. Here, the samples are heated (10 K/min) to a higher temperature (T_1), then cooled (30 K/min) and held at a lower temperature (T_2). The first sample was sintered at $T_1 = 950$ °C, $T_2 = 850$ °C and a dwelling time of 50 h. The ceramic body that resulted has a relative density of 92% and the grain size is between 0.6–2.8 μm. A second sample sintered at $T_1 = 970$ °C, $T_2 = 840$ °C and a dwelling time of 50 h achieved a relative density of 90% and a grain size interval of about 0.6–2 μm (Fig. 6e, f).

For comparative purposes, conventional sintering (dwelling time 1 h) of powder compacts of **2a** leads to ceramic bodies with a relative density of only 87% (5.24 g/cm^3) at 1,100 °C and to a density of 94% (5.68 g/cm^3) at 1,350 °C.

Powder diffraction patterns of ceramic bodies of **1a** after conventional sintering at different temperatures are shown in Fig. 7. Ceramic bodies sintered up to 1,200 °C consist of tetragonal $BaTiO_3$ and hexagonal $BaGeO_3$ [24]. Whereas sintering at 1,250 °C promotes the transformation from hexagonal to orthorhombic $BaGeO_3$ and hinders the reverse phase transition during the cooling stage [19], sintering considerably above 1,250 °C results in the formation of $Ba_2TiGe_2O_8$ [24, 30] and in a decrease of the orthorhombic $BaGeO_3$ phase.

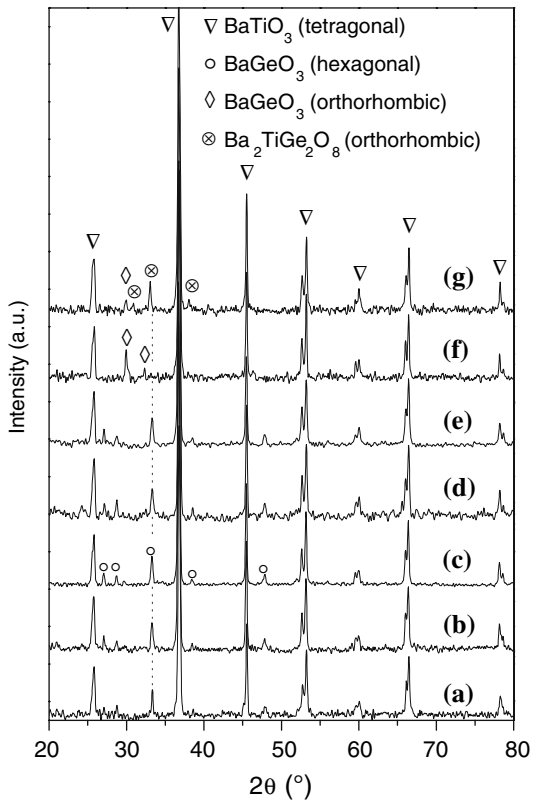

Fig. 7 XRD investigations on ceramic bodies of **1a** after different conventional sintering regimes (heating/cooling rate 10 K/min), (a) 900 °C, 10 h; (b) 950 °C, 5 h; (c) 1,100 °C, 1 h; (d) 1,150 °C, 1 h; (e) 1,200 °C, 1 h; (f) 1,250 °C, 1 h; (g) 1,350 °C, 1 h

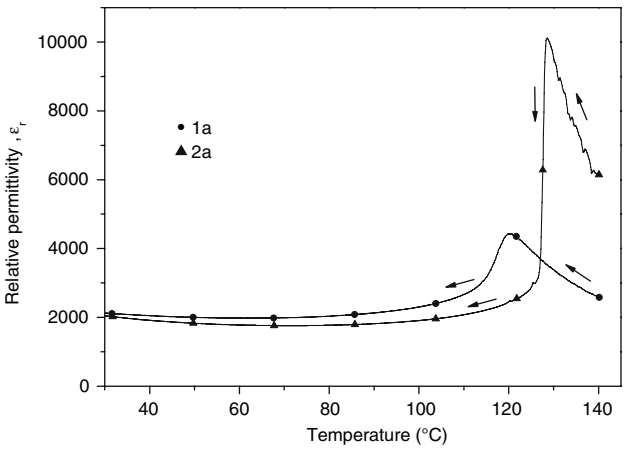

Fig. 8 Temperature dependence of the relative permittivity (ε_r) at 1 kHz of dense ceramic bodies **1a** and **2a**, respectively (sintered at 1,350 °C for 1 h). The figure shows the cooling curves (cooling rate 0.3 K/min)

The influence of the additive $BaGeO_3$ on the dielectric constant is represented in Fig. 8. The figure shows the temperature dependence of the dielectric constant (relative permittivity, ε_r) of $BaTiO_3$ (**2a**) and $Ba(Ti_{0.9}/Ge_{0.1})O_3$ (**1a**) ceramics after conventional sintering. The transition between the paraelectric and ferroelectric phase is shifted to lower temperatures by addition of $BaGeO_3$ (curve maxima: 128 °C (**2a**) and ca. 120 °C (**1a**)). Moreover, a reduction in the sharpness and the height of the curve, maximum of sample **1a** can be observed.

The cubic ⇆ tetragonal phase transition of $BaTiO_3$ was also analysed by dilatometric measurements of dense ceramic bodies after conventional sintering (Fig. 9). The

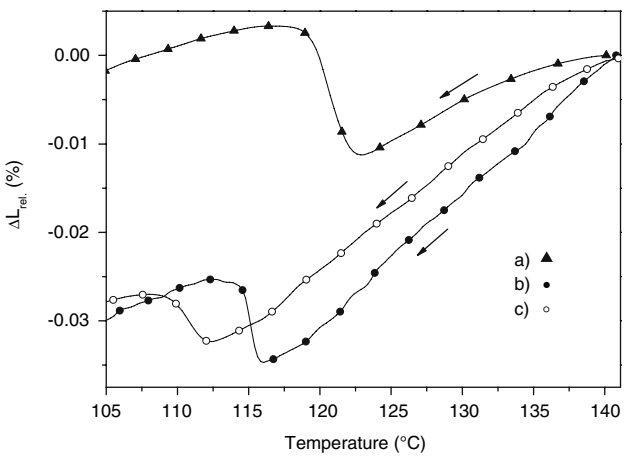

Fig. 9 Dilatometric measurements of the expansion of dense ceramic bodies during the cubic ⇆ tetragonal phase transition, (a) **2a** (1,350 °C, 1 h), (b) **1a** (1,350 °C, 1 h) and (c) **1a** (1,050 °C, 1 h). The figure shows the cooling curves (cooling rate 2.5 K/min, $\Delta L_{rel.} = \Delta L/L_0$)

phase transition temperature was determined at the points of inflection of the thermal expansion curve during the cooling phase. The phase transition temperature of a pure $BaTiO_3$ ceramic (**2a,** sintered at 1,350 °C) is 120.5 ± 0.3 °C. We observed a small shift to lower temperatures in $Ba(Ti_{0.9}/Ge_{0.1})O_3$ ceramics (**1a**). A ceramic body of **1a** sintered at 1,350 °C has a transition temperature of 115.4 ± 0.3 °C, whereas a sintering temperature of 1,050 °C leads to a transition temperature of 111.3 ± 0.3 °C.

Analogous observations were reported by Kuwabara et al. [38]. They noticed a shift of the Curie temperature in relation to the sintering temperature in pure $BaTiO_3$ ceramics.

Conclusion

Thermal decomposition of a solid solution of $[Ba(HOC_2H_4OH)_4][Ti_{0.9}Ge_{0.1}(OC_2H_4O)_3]$ (**1**) leads to a mixture of mainly $BaTiO_3$ and $BaGeO_3$ (denoted by $Ba(Ti_{0.9}/Ge_{0.1})O_3$). The final temperature for the formation of $Ba(Ti_{0.9}/Ge_{0.1})O_3$ depends on the heating rate, and is 716 °C with a heating rate of 1 K/min. A heating rate controlled calcination procedure of **1** leads to nm-sized $Ba(Ti_{0.9}/Ge_{0.1})O_3$ powder (**1a**) with a specific surface area of 16.9 m^2/g. Dilatometric investigations on powder compacts of **1a** reveal that the non-isothermal shrinkage starts at 790 °C and leads up to 1,170 °C to a relative bulk density of 96%. Dense ceramic bodies (relative density >90%) of **1a** can be obtained by conventional sintering at 900 °C and by a two-step sintering procedure with prolonged dwelling time at 850 °C. The final ceramics sintered to 1,250 °C consist of tetragonal $BaTiO_3$ and hexagonal/orthorhombic $BaGeO_3$, whereas higher sintering temperatures lead to the disappearance of the $BaGeO_3$ phase and to the formation of $Ba_2TiGe_2O_8$. Moreover, we observe a small decrease in the cubic ⇆ tetragonal phase transition temperature for $Ba(Ti_{0.9}/Ge_{0.1})O_3$ ceramics. The curve maximum of the dielectric constant (relative permittivity) is also shifted to a lower temperature and shows a reduction in sharpness and height.

Acknowledgements The authors thank Dr. Th. Müller for DTA, dilatometric and XRD measurements, and for his helpful discussions, Dr. U. Straube (Institute of Physics) for dielectric investigations and also Ms. Dipl.-Ing. (FH) C. Apfel (University of Jena) for thermoanalytic measurements. We are also grateful to Ms. M. Kelly for reading the manuscript. Financial support by the Federal State Saxony-Anhalt (Cluster of Excellence "Nanostructured Materials") is gratefully acknowledged.

References

1. Chaisan W, Yimnirun R, Ananta S (2007) Ferroelectrics 346:84
2. Kim HT, Han YH (2004) Ceram Int 30:1719
3. Yoon SO, Lung JH, Ki H (1991) Yoop Hakhoechi 28(5):359
4. Völtzke D, Abicht H-P (2000) Solid State Sci 2:149
5. Abicht H-P, Völtzke D, Schmidt H (1997) Mater Chem Phys 51:35
6. Pulvari CF (1959) J Am Ceram Soc 42(8):355
7. Baxter P, Hellicar NJ, Lewis B (1959) J Am Ceram Soc 42:465
8. Jeon H-P, Lee S-K, Kim S-W, Choi D-K (2005) Mater Chem Phys 94:185
9. Liu G, Roseman RD (1999) J Mater Sci 34:4439. doi: 10.1023/A:1004624918910
10. Payne DA, Park SM (1980) Heterophasic ceramic composition. U.S. Patent No. 4,218,723
11. Chu MS-H, Bultitude J, Hood C, Nimmo KL, Rand M (1996) Temperature stable dielectric. EU Patent No. EP 0,731,066,A1
12. Guha JP (1977) J Am Ceram Soc 60(5–6):246.
13. Guha JP, Kolar D (1972) J Mater Sci 7:1192. doi: 10.1007/BF00550202
14. Plessner KW, West R (1955) Proc Phys Soc B68:1150
15. Köferstein R, Jäger L, Lorenz V, Abicht H-P, Woltersdorf J, Pippel E, Görls H (2005) Solid State Sci 7:1280
16. Bode H, Claassen A, Jüstel B (1950) Handbuch der Analytischen Chemie, 3. Teil, Band IVb, Titan, Zirkon, Hafnium, Thorium, Springer-Verlag, Berlin, pp 82–98
17. Gmelins Handbuch der anorganischen Chemie – Germanium -, 8. Auflage, Ergänzungsband (1958) Verlag Chemie GmbH, Weinheim/Bergstrasse, p 465
18. Bieber B, Većera Z (1961) Coll Czech Chem Comm 26:2181
19. Köferstein R, Jäger L, Zenkner M, Abicht H-P (2007) Thermochim Acta 457:55
20. Birks LS, Friedman H (1946) J Appl Phys 17:687
21. Jäger L, Lorenz V, Wagner C, Müller T, Abicht H-P (2005) Z Kristallogr 220:183
22. Ischenko V, Woltersdorf J, Pippel E, Köferstein R, Abicht H-P (2007) Solid State Sci 9:21
23. Ischenko V, Woltersdorf J, Pippel E, Köferstein R, Abicht H-P (2007) Solid State Sci 9:303
24. PDF 2 (International Centre for Diffraction Data, Pennsylvania) $BaCO_3$ [5, 378], $BaTiO_3$ [72, $138_{tetragonal}$; 31-174_{cubic}], $BaGeO_3$ [30, $127_{hexagonal}$; 37-$137_{orthorhombic}$], Ba_2GeO_4 [39, 1257], $Ba_2TiGe_2O_8$ [44, 560]
25. Polotai AV, Ragulya AV, Tomila TV, Randall CA (2004) Ferroelectrics 298:243
26. Ragulya AV (1998) Nanostruct Mater 10(3):349
27. Garvie RC (1965) J Phys Chem 69(4):1238
28. Allred VD, Buxton SR, McBride JP (1957) J Chem Phys 61:117
29. Marks GW, Monson LA (1955) Ind Eng Chem 47(8):1611
30. Höche T, Esmaeilzadeh S, Uecker R, Lidin S, Neumann W (2003) Acta Cryst B59:209
31. Evans HT Jr (1961) Acta Cryst 14:1019
32. Demartin M, Herard C, Carry C, Lemaitre J (1997) J Am Ceram Soc 80(5):1079
33. M'Peko J-C, Portelles J, Rodriguez G (1997) J Mater Sci Lett 16:1850
34. Demartin M, Pethybridge G, Carry C (1993) 3rd European ceramic society conference, (Madrid, Spain), In: Duran P, Fernandez JF (ed) Vol 1. Faenza Editrice Iberica, Spain, pp 787–792
35. Sudre O, Lange FE (1992) J Am Ceram Soc 75(12):3241
36. Balzer B, Hagemeister M, Kocher P, Gaukler LJ (2004) J Am Ceram Soc 87(10):1932
37. Chen I-W, Wang X-H (2000) Nature 404:168
38. Kuwabara M, Matsuda H, Kurata N, Matsuyama E (1997) J Am Ceram Soc 80(10):2590